Mechanistic Studies of Stereospecific Polymerization of Methacrylates Using a Cationic, Chiral *ansa*-Zirconocene Ester Enolate

Antonio Rodriguez-Delgado and Eugene Y.-X. Chen*

Department of Chemistry, Colorado State University, Fort Collins, Colorado 80523-1872

Received December 22, 2004; Revised Manuscript Received January 27, 2005

ABSTRACT: Mechanistic studies of isospecific polymerization of methacrylates by a cationic, chiral *ansa*-zirconocene ester enolate complex, *rac*-(EBI)Zr^+(THF)[OC(O^{i}Pr)=CMe_2][MeB(C_6F_5)$_3$]$^-$ [**1**; EBI = C_2H_4-(Ind)$_2$], are reported. Complex **1** effects isospecific and living (co)polymerization of methyl methacrylate (MMA) and *n*-butyl methacrylate (BMA), producing highly isotactic homopolymers and block copolymers with narrow molecular weight distributions and high initiator efficiencies. Investigations of statistical copolymerizations of MMA and BMA have yielded monomer reactivity ratios of $r_{MMA} = 0.62$ and $r_{BMA} = 0.72$ (the Kelen−Tüdõs method), indicating that the copolymer formed instantaneously has a somewhat alternating character. Studies of MMA polymerization kinetics have shown that propagation is first order in both concentrations of the monomer and the active species. The single MMA addition product, *rac*-(EBI)ZrMe[OC(OMe)=C(Me)CH_2C(Me_2) C(O^{i}Pr)=O] (**3**), has been isolated from the reaction between the neutral *rac*-(EBI)ZrMe[OC(O^{i}Pr)=C(Me_2)] (**2**) and MMA; however, subsequent MMA additions do not proceed, unless the single addition product is further treated with B(C_6F_5)$_3$ to generate the eight-membered-ring cyclic ester enolate species, *rac*-(EBI)Zr^+[OC(OMe)=C(Me)CH_2C(Me_2)C(O^{i}Pr)=O][MeB-(C_6F_5)$_3$]$^-$ (**4**), which corresponds to the structure of the intermediate for the single MMA addition product of **1**. All results presented here are consistent with the conclusion that isospecific polymerization of methacrylates by **1**—which models the proposed isospecific propagating species for the methacrylate polymerization by chiral *ansa*-zirconocene complexes—is enantiomorphic site controlled and proceeds in a monometallic, intramolecular Michael addition mechanism.

Introduction

Polymerization of methacrylates by group 4 metallocene and related complexes[1−7] has attracted increasing attention due to the following important attributes of this polymerization: (1) there is a paradigm shift in terms of scientific curiosity on utilizing highly active, electrodeficient transition-metal complexes for polymerization of polar monomers; (2) group 4 metallocene complexes with considerably diverse structural motifs are readily, and in many cases commercially, available, thanks to comprehensive studies of their roles in coordination polymerization of nonpolar olefins; and (3) these complexes, when used in a suitable initiating form (e.g., ester enolates), typically exhibit a high degree of control over polymerization, especially the stereochemistry of polymerization.

Collins and co-workers showed that a two-component system consisting of an *achiral* neutral zirconocene ester enolate complex, Cp_2ZrMe[OC(O^{t}Bu)=CMe_2], as initiator, and a cationic zirconocene complex, [Cp_2ZrMe-(THF)]$^+$[BPh_4]$^-$, as catalyst, polymerizes methyl methacrylate (MMA) in a living fashion to syndiotactic-rich poly(methyl methacrylate) (PMMA).[1j] The mechanistic studies[1f,j] revealed a group-transfer-type[8] *bimetallic* propagation involving the rate-limiting, intermolecular Michael addition of the zirconocene enolate to the activated MMA by the cationic zirconocene (Scheme 1). Both monometallic and bimetallic mechanisms were initially considered and studied by Collins and co-workers,[1j] using appropriate cationic and neutral enolate precursors, and later examined theoretically by Sustmann and co-workers,[7c] although in the parent [Cp_2Zr] system, the bimetallic pathway is more competitive.

* Corresponding author. E-mail: eychen@lamar.colostate.edu.

Scheme 1

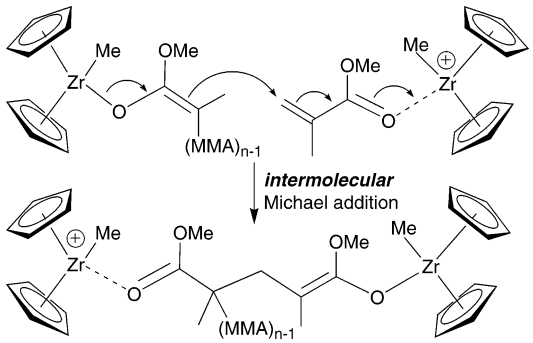

Regarding the mechanism for the stereospecific MMA polymerization by *chiral ansa*-zirconocene complexes, Collins and co-workers[2o] suggested 10 years ago, based on the experiments with *rac*- vs optically pure *ansa*-zirconocene alkyl initiators, that the propagation mechanism may be different than the bimetallic mechanism established for the two-component, achiral system mentioned above. Marks and co-workers[2l] employed the isolated μ-Me dinuclear metallocenium initiators which could potentially function by either the bimetallic or monometallic mechanism. Höcker and co-workers[2h] investigated the kinetics of isospecific MMA polymerization using a chiral, C_1-symmetric *ansa*-zirconocene alkyl initiator, [Me_2CCp(Ind)ZrMe(THF)]$^+$[BPh_4]$^-$; the kinetic results were fitted to a monometallic mechanism in which a fast associative active-site epimerization occurs after each propagating step (i.e., monomer addition always takes place on the same lateral coordination site of the Zr center[6d]). However, the alkyl complex used for this study is not the active propagating species, and slow initiation and termination reactions can complicate the polymerization and kinetic results. Fur-

10.1021/ma047345c CCC: $30.25
Published on Web 03/08/2005

Scheme 2

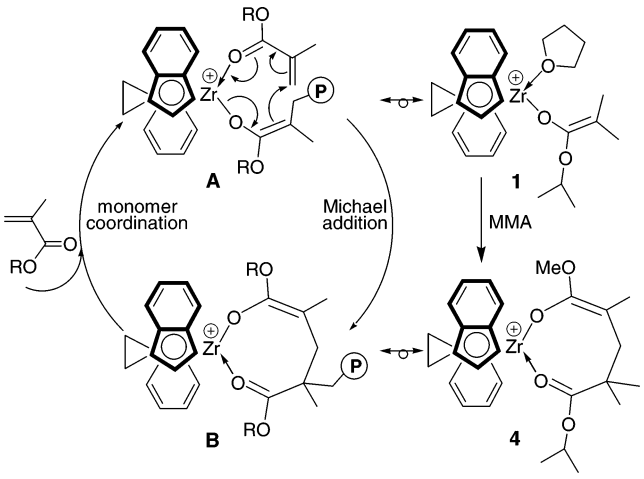

thermore, mechanistic studies of isospecific polymerization of methacrylates using chiral, C_2-symmetric *ansa*-zirconocene complexes have been a challenge because of the synthetic difficulty in isolating the cationic *ansa*-zirconocene *ester enolate* that models the proposed active propagating species.[2a,6d]

We[2a] recently reported the synthesis and structure of chiral *ansa*-zirconocene mono- and bis-ester enolates as well as the isolation of the cationic, chiral *ansa*-zirconocene ester enolate complex *rac*-(EBI)Zr^+(THF)[OC(O^{i}Pr)=CMe_2][$MeB(C_6F_5)_3$]$^-$ (**1**) (Scheme 2). Complex **1** is highly active and isospecific for the well-controlled polymerization of methacrylates. The central objective of the present study was to carry out mechanistic studies of isospecific polymerization of methacrylates using this well-characterized, cationic chiral *ansa*-zirconocene ester enolate that models the proposed active, isospecific propagating species **A** (Scheme 2). Our current studies have conclusively shown that the MMA polymerization by the cationic, chiral *ansa*-zirconocene ester enolate **1** is enantiomorphic-site controlled and proceeds in a *monometallic*, intramolecular Michael addition mechanism via cyclic ester enolate intermediate (resting state) **B** which is simulated by the isolated cyclic ester enolate complex **4** (Scheme 2). This mechanism resembles that proposed by Yasuda and coworkers[9] for the MMA polymerization initiated by isoelectronic, neutral lanthanocenes.

Experimental Section

Materials and Methods. All syntheses and manipulations of air- and moisture-sensitive materials were carried out in flamed Schlenk-type glassware on a dual-manifold Schlenk line, a high-vacuum line (10^{-5}−10^{-7} Torr), or an argon-filled glovebox (<1.0 ppm oxygen and moisture). NMR-scale reactions (typically in a 0.02 mmol scale) were conducted in Teflon-valve-sealed J. Young-type NMR tubes. HPLC grade organic solvents were first saturated with nitrogen during filling the solvent reservoir and then dried by passage through activated alumina (for Et_2O, THF, and CH_2Cl_2) followed by passage through Q-5-supported copper catalyst (for toluene and hexanes) stainless steel columns. Benzene-d_6, toluene-d_8, and THF-d_8 were dried over sodium/potassium alloy and vacuum-distilled or filtered, whereas C_6D_5Br, $CDCl_3$, and CD_2Cl_2 were dried over activated Davison 4 Å molecular sieves. NMR spectra were recorded on either a Varian Inova 300 (FT 300 MHz, ^{1}H; 75 MHz, ^{13}C; 282 MHz, ^{19}F) or a Varian Inova 400 spectrometer. Chemical shifts for ^{1}H and ^{13}C spectra were referenced to internal solvent resonances and are reported as parts per million relative to tetramethylsilane, whereas ^{19}F NMR spectra were referenced to external $CFCl_3$. Elemental analyses were performed by Desert Analytics, Tucson, AZ.

Methyl methacrylate (MMA) and *n*-butyl methacrylate (BMA) were purchased from Aldrich Chemical Co. The monomers were first degassed and dried over CaH_2 overnight, followed by vacuum distillation, and final purification involved titration with neat tri(*n*-octyl)aluminum to a yellow end point[10] followed by distillation under reduced pressure. The purified monomers were stored in a −30 °C glovebox freezer. 2,6-Di-*tert*-butyl-4-methylphenol (butylated hydroxytoluene, BHT-H) was purchased from Aldrich Chemical Co. and recrystallized from hexanes prior to use.

Tris(pentafluorophenyl)borane, $B(C_6F_5)_3$, was obtained as a research gift from Boulder Scientific Co. and further purified by recrystallization from hexanes at −35 °C. The $(C_6F_5)_3B$·THF adduct was prepared by addition of THF to a toluene solution of the borane followed by removing the solvents and drying in vacuo. Neutral chiral *ansa*-zirconocene ester enolate *rac*-(EBI)ZrMe[OC(O^{i}Pr)=CMe_2] (**2**) and cationic ester enolate *rac*-(EBI)Zr^+(THF)[OC(O^{i}Pr)=CMe_2][$MeB(C_6F_5)_3$]$^-$ (**1**) were prepared according to literature procedures.[2a] Complex **1** can also be cleanly and quantitatively generated via in situ mixing of **2** with $(C_6F_5)_3B$·THF in CH_2Cl_2 at room temperature.

Isolation of *rac*-(EBI)ZrMe[OC(OMe)=C(Me)CH_2C(Me$_2$)C(O^{i}Pr)=O] (3) from the Reaction of Neutral Enolate 2 with MMA. In an argon-filled glovebox, a 30 mL glass reactor was charged with 100 mg (0.203 mmol) of **2**, 20.4 mg (0.203 mmol) of MMA, and 10 mL of CH_2Cl_2. The resulting bright yellow solution was stirred for 3 h at ambient temperature, after which the solvent was removed in vacuo affording a sticky yellow oil. This oily product was redissolved in 4 mL of hexanes and stored at −30 °C for 2 days. No solids or crystals were observed, so the solution was concentrated to one-half of its volume. The concentrated solution was left in a freezer inside the glovebox at −30 °C for 16 h, yielding a yellow microcrystalline solid. The yellow solid collected after filtration was dried to give 0.048 g of the first crop of the product. Subsequent concentration of the filtrate and recrystallization yielded an additional 0.041 g of the product. The total yield was 0.089 g (74%). Anal. Calcd for $C_{33}H_{40}O_4Zr$: C, 66.90; H, 6.82. Found: C, 66.19; H, 6.53.

^{1}H NMR (C_6D_6, 23 °C) for **3**: δ 7.32−6.84 (m, 8H), 6.31 (d, J = 3.1 Hz, 1H), 6.07 (d, J = 3.1 Hz, 1H), 6.05 (d, J = 3.1 Hz, 1H), 5.56 (d, J = 3.1 Hz, 1H), 5.09 (sept, J = 6.3 Hz, 1H, C*H*Me$_2$), 2.99 (s, 3H, O*Me*), 2.88−2.52 (m, 4H, CH_2CH_2), 2.64 and 2.56 (dd, 1H each, C*H*$_2$), 1.41 (s, 3H, =C*Me*), 1.38 (d, J = 3.9 Hz, 6H, C*Me*$_2$), 1.12 (d, J = 6.3 Hz, 6H, CH*Me*$_2$), −0.58 (s, 3H, Zr−*Me*). ^{1}H NMR (CD_2Cl_2, 23 °C) for comparison: δ 7.76 (d, J = 8.8 Hz, 1H), 7.46 (d, J = 8.8 Hz, 1H), 7.34−7.05 (br, 6H), 6.47 (d, J = 3.2 Hz, 1H), 6.36 (br, J = 3.2 Hz, 1H), 5.91 (br, 2H), 4.91 (sept, J = 6.4 Hz, 1H, C*H*Me$_2$), 3.77−3.42 (m, 4H, CH_2CH_2), 2.94 (s, 3H, O*Me*), 2.12 and 2.08 (dd, 1H each, C*H*$_2$), 1.22 (d, J = 4 Hz, 6H, C*Me*$_2$), 1.15 (b, 9H, CH*Me*$_2$ and =C*Me*), −0.92 (s, 3H, Zr −*Me*). ^{13}C NMR (C_6D_6, 23 °C): δ 177.65 [*C*(O^{i}Pr)=O], 157.51[O*C*(OMe)=], 127.09, 126.98, 125.91, 124.81, 124.70, 124.63, 124.05, 123.70, 122.68, 122.03, 121.84, 120.46, 118.75, 115.49, 113.74, 111.57, 105.20, 103.27 (18 resonances for Ind-ring carbons), 82.51 (=*C*Me), 66.79 (O*C*HMe$_2$), 54.31 (O*C*H$_3$), 42.96 (*C*Me$_2$), 42.35 (*C*H$_2$), 31.82 (Zr−Me), 28.16 (CH_2CH_2), 27.17 (CH_2CH_2), 25.79 (C*Me*$_2$), 21.69 (CH*Me*$_2$), 16.91(=C*Me*).

Isolation of *rac*-(EBI)Zr^+[OC(OMe)=C(Me)CH_2C(Me$_2$)C(O^{i}Pr)=O][$MeB(C_6F_5)_3$]$^-$ (4): the Single MMA Addition Product of 1. In an argon-filled glovebox, a 30 mL glass reactor was charged with 30 mg (0.050 mmol) of **3** and 5 mL of CH_2Cl_2. Into a second 20 mL glass reactor was placed 29.5 mg (0.050 mmol) of $(C_6F_5)_3B$·THF and 5 mL of CH_2Cl_2; this solution was then added to the stirred solution of **3** via pipet at ambient temperature. The color of the resulting mixture changed instantaneously from bright yellow to dark orange. The solution was stirred for 15 min, after which the volatiles were removed in vacuo to afford a viscous orange-red oil. This crude product was washed repeatedly with hexanes (5 × 4 mL) and dried to give 0.044 g (81%) of the pure product as an

orange solid. Several attempts to grow single crystals of **4** were unsuccessful. Anal. Calcd for $C_{51}H_{40}BF_{15}O_4Zr$: C, 55.44; H, 3.65. Found: C, 55.23; H, 3.83.

^{1}H NMR (CD_2Cl_2, 23 °C) for **4**: δ 8.07 (d, J = 8.4 Hz, 1H), 7.96 (d, J = 8.4 Hz, 1H), 7.38−7.23 (m, 6H), 6.31 (d, J = 3.3 Hz, 1H), 6.28 (d, J = 3.3 Hz, 1H), 6.22 (d, J = 3.3 Hz, 1H), 5.95 (d, J = 3.3 Hz, 1H), 4.34 (sept, J = 6.4 Hz, 1H, C*H*Me$_2$), 4.11−3.99 (m, 4H, CH_2CH_2), 3.14 (s, 3H, O*Me*), 2.28−2.20 (m, 2H, C*H*$_2$), 1.51 (s, 3H, =C*Me*), 1.42 (s, 6H, C*Me*$_2$), 1.31 (d, J = 6.3 Hz, 6H, CH*Me*$_2$), 0.54 (s, br, 3H, B−*Me*). ^{19}F NMR (CD_2Cl_2, 23 °C): δ −131.43 (d, $^3J_{F-F}$ = 19.5 Hz, 6F, *o*-F), −163.54 (t, $^3J_{F-F}$ = 19.5 Hz, 3F, *p*-F), −166.29 (m, 6F, *m*-F).^{13}C NMR (CD_2Cl_2, 23 °C): δ 192.37 [*C*(O^{i}Pr)=O], 153.72 [O*C*(OMe)=], 128.26, 128.09, 127.77, 127.31, 127.07, 126.29, 125.93, 124.42, 124.09, 123.67, 123.40, 122.74, 121.23, 118.11, 116.91, 116.34, 106.53, 104.04 (18 resonances for Ind-ring carbons; carbons for the C_6F_5 groups omitted due to C−F coupling), 82.45 (=*C*Me), 77.04, 71.39, 43.93, 40.18, 30.27, 26.19 and 24.15 (*CH*$_2$*CH*$_2$), 21.91 and 20.80 (OCH*Me*$_2$), 17.07 (=C*Me*), 9.95 (B−*Me*).

General Polymerization Procedures. Polymerizations were performed either in 30 mL, oven- and flame-dried vacuum flasks inside the glovebox or in 25 mL oven- and flame-dried Schlenk flasks interfaced to the dual-manifold Schlenk line. In a typical procedure, a 2.5 mL stock solution of **2** (23.3 μmol) in CH_2Cl_2 was mixed in a flask with a solution of $(C_6F_5)_3B$·THF (23.3 μmol) in 2.5 mL of CH_2Cl_2 and stirred for 10 min to cleanly generate the cationic zirconocene ester enolate **1**. MMA (1.00 mL, 9.35 mmol) or BMA (1.48 mL, 9.35 mmol) was quickly added via pipet (for polymerizations in the glovebox) or gastight syringe (for polymerizations on the Schlenk line), and the sealed flask was kept with vigorous stirring at the preequilibrated bath temperature. For block copolymerizations, a second portion of MMA or BMA was added after the completion of the first block, and the polymerization was continued. For statistical copolymerization of MMA and BMA, a mixture of MMA/BMA with predetermined molar ratios of 80/20, 70/30, 60/40, 50/50, and 20/80 was added to a solution of **1** in a $[MMA + BMA]_0/[\mathbf{1}]_0$ = 1000/1. After the measured time interval, the polymerization was quenched by the addition of 5 mL of 5% HCl-acidified methanol. The statistical copolymerizations were quenched at low conversions (ca. <5%). The quenched mixture was precipitated into 100 mL of methanol, stirred for 1 h, filtered, washed with methanol, and dried in a vacuum oven at 50 °C overnight to a constant weight.

Polymerization Kinetics. Kinetic experiments were carried out in stirred Schlenk flasks at 23 °C using the similar procedure as already described above, except that, at appropriate time intervals, 0.2 mL aliquots were withdrawn from the reaction mixture using syringe and quickly quenched into 1 mL vials containing 0.6 mL of undried "wet" $CDCl_3$ stabilized with 250 ppm of BHT-H. The quenched aliquots were analyzed by ^{1}H NMR. The ratio of $[MMA]_0$ to $[MMA]_t$ at a given time t, $[MMA]_0/[MMA]_t$, was determined by integration of the peaks for MMA (5.2 and 6.1 ppm for the vinyl signals; 3.4 ppm for the OMe signal) and PMMA (centered at 3.4 ppm for the OMe signals) according to $[MMA]_0/[MMA]_t = 2A_{3.4}/3A_{5.2+6.1}$, where $A_{3.4}$ is the total integrals for the peaks centered at 3.4 ppm (typically in the region 3.2−3.6 ppm) and $A_{5.2+6.1}$ is the total integrals for both peaks at 5.2 and 6.1 ppm. Apparent rate constants (k_{app}) were extracted from the slope of the best fit line to the plot of $\ln([MMA]_0/[MMA]_t)$ vs time.

Polymer Characterizations. The low-molecular-weight PMMA sample was analyzed by matrix-assisted laser desorption/ionization time-of-flight mass spectroscopy (MALDI−TOF MS); the experiment was performed on an Ultraflex MALDI−TOF mass spectrometer (Bruker Daltonics) operated in linear, delayed extraction, positive ion mode using a Nd:YAG laser at 355 nm and 25 kV accelerating voltage. A thin layer of a 1% NaI solution was first deposited on the target plate, followed by 1 μL of both sample and matrix (dithranol, 10 mg/mL in THF).

Glass transition temperatures (T_g) of the polymers were measured by differential scanning calorimetry (DSC) on a DSC 2920, TA Instrument. Samples were first heated to 180 °C at 20 °C/min, equilibrated at this temperature for 4 min, and cooled to −40 °C at 20 °C/min. After being held at this temperature for 4 min, the samples were then reheated to 180 °C at 10 °C/min. All T_g values were obtained from the second scan, after removing the thermal history. Polymer molecular weights and molecular weight distributions were measured by gel permeation chromatography (GPC) analyses carried out at 40 °C, at a flow rate of 1.0 mL/min, and with THF as the eluent, on a Waters University 1500 GPC instrument. The instrument was calibrated with 10 PMMA standards, and chromatograms were processed with Waters Empower software. ^{1}H NMR spectra for the analysis of PMMA and PBMA microstructures were recorded in $CDCl_3$ and analyzed according to the literature.[6a,11]

Results and Discussion

The isolated cationic, chiral *ansa*-zirconocene ester enolate complex **1**[2a] is highly active and isospecific for polymerization of methacrylates, and this polymerization initiated by **1** occurs in a living fashion and is enantiomorphic-site controlled ($2[rr]/[mr]$ = 1.0). To simplify the polymerization kinetics experimental procedures, we investigated the possibility of in situ generation of **1**. Indeed, the instantaneous, clean, and quantitative generation of **1** was achieved upon mixing of the neutral methyl zirconocene ester enolate **2** with $(C_6F_5)_3B$·THF in CH_2Cl_2 at room temperature (Scheme 3). Complex **1** is stable in a solution of CH_2Cl_2 (which is the solvent used in the polymerization kinetic studies) at room temperature, and no decomposition was detected over a period of 6 h at room temperature. (Note that the polymerization time scale of the present study is typically less than 30 min.) Subsequently, the in situ generated cation **1** in CH_2Cl_2 was used for MMA polymerization kinetic studies.

Scheme 3

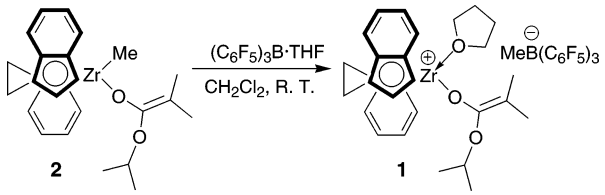

It is important to point out that the remarkable ambient-temperature stability/isolability of the cationic ester enolate **1** and its high efficacy as initiator appear to be a result of combinations of right choices of alkyl ester enolate, bridged indenyl ancillary, and external donor ligands. In the absence of a donor ligand such as THF, the cationic zirconocene ester enolate species decomposes rapidly.[2a] Cationic zirconocene *tert*-butyl ester enolate complexes decompose at ambient or subambient temperatures, even in the presence of THF, to carboxylate complexes via elimination of isobutylene.[1a,b,6d] After many prior attempts, we finally resided at the isopropyl isobutyrate ligand for its combined sterics and electronics to effectively prevent the potential formation of dimeric zirconocene ester enolates and elimination of an alkene, although the latter process does occur when the strongly Lewis acid $Al(C_6F_5)_3$ is used in the reaction.[2a] Furthermore, even with the isopropyl isobutyrate ligand and in the presence of THF, the cationic titanium ester enolate complex with the "constrained geometry" ligation is not isolable at ambient temperature.[6a]

MMA Polymerization Results and Kinetics. Typical results of MMA polymerization by **1** in CH_2Cl_2 at 23 °C are summarized in Table 1. As shown in Table 1,

Table 1. MMA Polymerization Results by Cationic, Chiral Zirconocene Ester Enolate Complex 1[a]

run no.	[**1**] (mmol/L)	$[MMA]_0/[\mathbf{1}]_0$	time (min)	conv (%)	$10^4 M_n$[b] (g/mol)	PDI[b] (M_w/M_n)	I^*[c] (%)	[*mm*][d] (%)
1	4.66	400	1	35	1.62	1.04	0.86	95
2			2	54	2.52	1.04	0.87	
3			2.5	62	3.20	1.04	0.76	
4			3	70	3.49	1.05	0.80	
5			4	79	3.88	1.05	0.81	
6			5	87	4.35	1.05	0.80	
7			6	92	4.40	1.05	0.84	95
8	3.73	500	1	32	1.76	1.04	0.90	95
9			2	50	3.00	1.04	0.83	
10			3	64	3.80	1.05	0.84	
11			3.5	70	4.22	1.04	0.83	
12			4	75	4.37	1.05	0.85	
13			5	80	4.43	1.06	0.90	
14			6	86	4.76	1.06	0.90	
15			8	93	4.97	1.07	0.93	95
16	3.11	600	1.5	27	2.34	1.05	0.69	93
17			3	51	3.86	1.05	0.79	
18			4	61	4.56	1.05	0.80	
19			6	71	5.12	1.07	0.83	
20			8	86	6.04	1.07	0.85	
21			12	95	6.70	1.08	0.85	93
22	2.32	800	1	14	1.45	1.05	0.77	94
23			2	29	2.47	1.04	0.93	
24			3	43	4.16	1.05	0.82	
25			4	52	4.78	1.06	0.87	
26			12	78	6.64	1.09	0.93	
27			15	89	6.83	1.08	0.96	
28			20	92	7.06	1.09	0.96	94
29	1.87	1000	1	12	1.70	1.04	0.70	93
30			2	25	3.28	1.04	0.76	
31			3	36	4.70	1.04	0.76	
32			4	44	5.61	1.04	0.78	
33			8	70	8.69	1.05	0.80	
34			10	78	9.60	1.08	0.81	
35			12	84	9.61	1.05	0.87	
36			15	88	10.49	1.06	0.83	93
37	1.24	1500	2	22	3.84	1.04	0.85	
38			4	31	6.78	1.05	0.70	
39			8	54	9.21	1.09	0.88	
40			12	70	13.44	1.06	0.78	
41			15	74	14.27	1.11	0.77	
42			20	78	14.54	1.12	0.80	
43			25	79	14.76	1.13	0.80	

[a] All polymerizations were carried out in flame-dried Schlenk flasks on a Schlenk line using an external temperature-control bath set at 23 °C. [b] Number-average molecular weight (M_n) and polydispersity index (PDI) determined by GPC relative to PMMA standards. [c] Initiator efficiency (I^*) = M_n(calcd)/M_n(exptl), where M_n(calcd) = MW(MMA) × $[MMA]_0/[\mathbf{1}]_0$ × conversion (%). [d] Isotacticity ([*mm*] methyl triad distribution) determined by ^{1}H NMR spectroscopy.

the polymerizations of MMA by **1** in $[MMA]_0/[\mathbf{1}]_0$ ratios = 400−1000 are rapid and produce PMMA with high isotacticity ([*mm*] = 93−95%), small polydispersity indices (PDI = M_w/M_n = 1.04−1.09), and initiator efficiencies (I^*) from moderate 70% to high 96%. For the polymerization with a higher $[MMA]_0/[\mathbf{1}]_0$ ratio (i.e., 1500), there is a slight increase of the PDI value up to 1.13 in the high monomer conversion (>74%) regime. Nevertheless, several lines of evidence, including the aforementioned polymerization results, the production of the well-defined block copolymer of PMMA-*b*-PBMA with a small PDI value of 1.03 (vide infra), and the observed linear increase of the polymer M_n with $[MMA]_0/[\mathbf{1}]_0$ ratios and with monomer conversion, which is coupled with the small, nearly constant PDI values (Figure 1), clearly show living characteristics of this polymerization.

To further confirm the living nature of this polymerization and also identify the initiation and termination

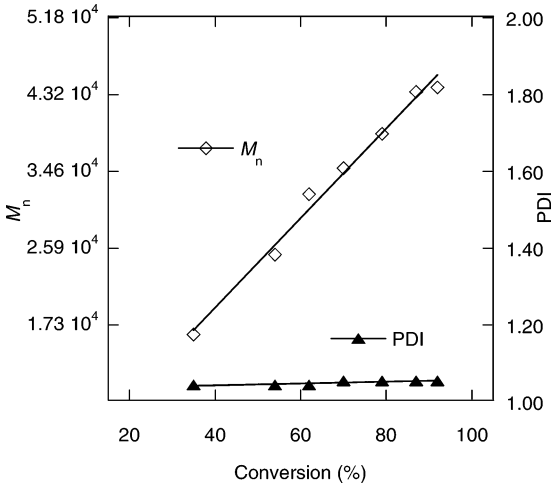

Figure 1. Plot of M_n and PDI of PMMA by **1** {$[MMA]_0/[\mathbf{1}]_0$ = 400; 23 °C} vs monomer conversion.

chain-end groups, the low-molecular-weight PMMA produced by **1** was characterized by MALDI−TOF mass spectrometry (Figure 2). The plot of *m/z* values of the major set of peaks in the MALDI−TOF mass spectrum vs the number of MMA repeat units yielded a straight line, giving a slope of 100.02 and an intercept of 153.73 (Figure 3); the slope corresponds to the mass of the MMA monomer, whereas the intercept is the sum of the masses of Na^+ (from the added NaI) and the end groups which correspond to a formula of $C_7H_{14}O_2$. This analysis clearly shows that the polymer has a structural formula of [^{i}PrOC(=O)C(Me_2)−$(MMA)_n$−H], where the initiation chain end [^{i}PrOC(=O)C(Me_2)−] is derived from the initiating isopropyl isobutyrate group present in complex **1** and the termination chain end (H) from HCl-acidified methanol during the workup procedure. In Figure 2 there also exists a minor series of peaks with the *m/z* value of each peak differing from the major peak by 42 (C_3H_6). A similar plot to Figure 3, but using the minor peaks, yielded the same slope but a different intercept of 111.87, corresponding to a polymer structural formula of [HOC(=O)C(Me_2)−$(MMA)_n$−H]·Na^+, where the chain end group [HOC(=O)C(Me_2)−] is presumably resulted from the acid-catalyzed loss of the isopropyl group during the workup procedure.

Results of the polymerization kinetic studies using complex **1** generated in situ from the reaction of **2** and $(C_6F_5)_3B$·THF at 23 °C in CH_2Cl_2 (vide supra) and with $[MMA]_0/[\mathbf{1}]_0$ ratios from 400 to 1500 clearly showed that propagation is first order in [MMA] for all the $[MMA]_0/[\mathbf{1}]_0$ ratios investigated in this study (Figure 4). A double-logarithm plot (Figure 5) of the apparent rate constants (k_{app}), which were obtained from the slopes of the best-fit lines to the plots of $\ln([MMA]_0/[MMA]_t)$ vs time, as a function of [**1**] was fit to a straight line (R^2 = 0.997) of slope = 1.1(1). The kinetic order with respect to [**1**], given by the slope of 1.1(1), reveals that propagation is also first order in [Zr], indicating a *monometallic* propagation mechanism.

Block and Random Copolymerizations of MMA with BMA and Monomer Reactivity Ratios. Sequential block copolymerization of MMA and BMA by **1** in CH_2Cl_2 at 23 °C with a ratio of $[MMA]_0/[BMA]_0/[\mathbf{1}]_0$ = 500/500/1 afforded the well-defined block copolymer PMMA-*b*-PBMA in quantitative yield (Table 2). The initiator efficiency of the block copolymerization starting from MMA polymerization (30 min) followed by BMA

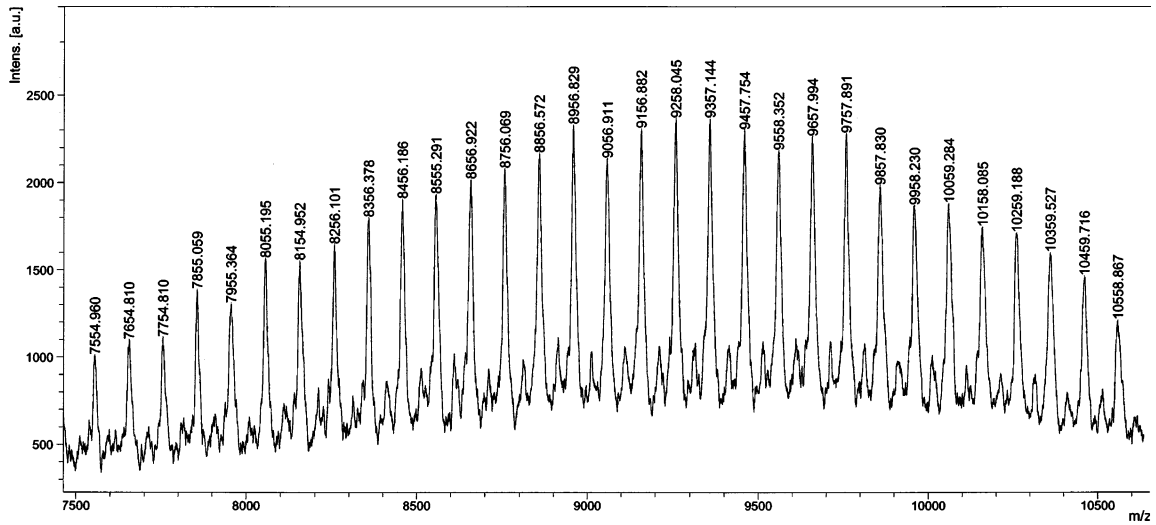

Figure 2. Portion of the MALDI−TOF mass spectrum of the low-molecular-weight PMMA produced by **1** at 23 °C in CH_2Cl_2.

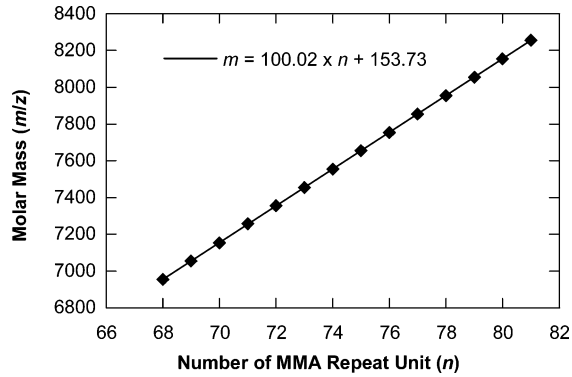

Figure 3. Plot of *m/z* values from the MALDI−TOF spectrum vs the number of MMA repeat units (n).

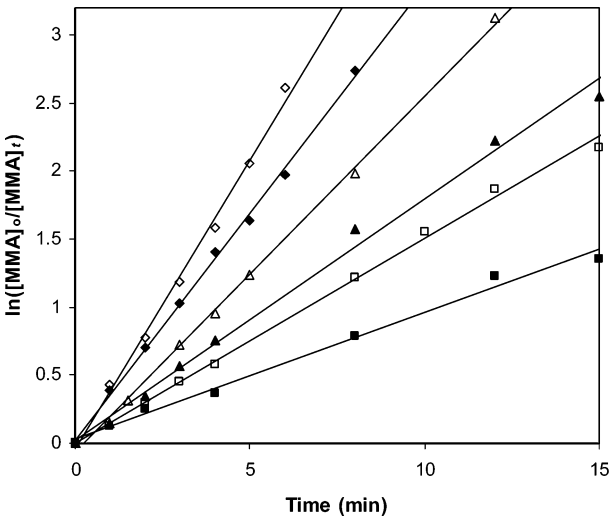

Figure 4. Semilogarithmic plots of $\ln\{[MMA]_0/[MMA]_t\}$ vs time for the polymerization of MMA by **1** in CH_2Cl_2 at 23 °C. Conditions: $[MMA]_0 = 1.87$ M, $[\mathbf{1}]_0 = 4.66$ mM (◇), 3.73 mM (◆); 3.11 mM (△), 2.32 mM (▲), 1.87 mM (□), and 1.24 mM (■).

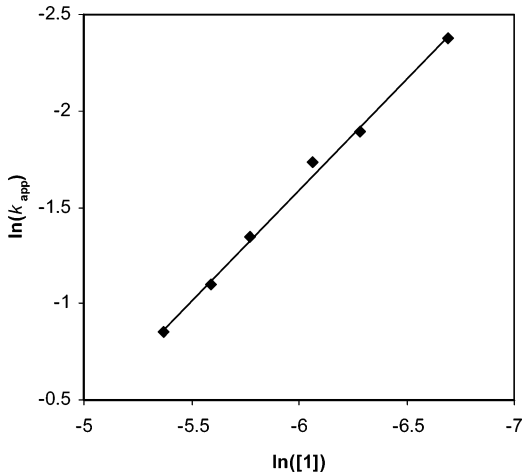

Figure 5. Plot of $\ln(k_{app})$ vs ln[**1**] for the MMA polymerization by **1** in CH_2Cl_2 at 23 °C.

polymerization (45 min) was 81%, and the block copolymer showed a single sharp peak on the GPC trace with PDI = 1.03 (run 1, Table 2). Both blocks are highly isotactic, with collective isotacticity of $[mm] = 94\%$; this is an overall value accounting for both blocks because of an overlap in the methyl triad region of PMMA and PBMA. The isotactic block copolymer PMMA-*b*-PBMA exhibits two distinct T_g's characteristic of each of the component segments (i.e., $T_g(1) = 62$ °C for the *i*-PMMA block and $T_g(2) = -11$ °C for the *i*-PBMA block, Scheme 4). The molar composition of the two monomer units in the block copolymer obtained from the ^{1}H NMR analysis is the same as the monomer molar feed ratio (i.e., 1:1), upon quantitative monomer conversion. The well-defined diblock copolymer was also prepared from sequential copolymerization starting from polymerization of BMA (run 2, Table 2). The isotactic PBMA-*b*-PMMA block copolymer obtained from this sequence is almost the same as PMMA-*b*-PBMA, except for a higher initiator efficiency of 86% and a small variation in T_g values for both blocks. This experiment further confirms that both PMMA and PBMA polymer chains initiated by **1** are living under the conditions employed in this study.

Statistical copolymerizations of MMA and BMA were carried out in a fixed [MMA + BMA]/[**1**] ratio of 1000/1 but varied feed ratios of [MMA]/[BMA] = 80/20, 70/30, 60/40, 50/50, and 20/80. To satisfy the differential copolymerization equation for determination of monomer reactivity ratios, all copolymerization reactions were quenched at low conversions (ca. <5%).[12] The composition of the copolymers was determined by ^{1}H NMR,[6a] and the results were processed using both the Fineman−Ross[13] linearization and the Kelen−Tüdõs[14]

Table 2. MMA and BMA Copolymerization Results by Chiral Zirconocenium Ester Enolate 1[a]

run no.	[**1**] (mM)	$[MMA]_0/[BMA]_0/[\mathbf{1}]_0$	time (min)	conv (%)	10^4M_n(exptl)	PDI (M_w/M_n)	10^4M_n(calcd)	I^* (%)	[*mm*] (%)
1	3.73	500:500:1	30, 45	>99	15.0	1.03	12.1	0.81	94
2	3.73	500:500:1	45, 30	>99	14.0	1.04	12.1	0.86	94

[a] See Table 1 footnotes for explanations of parameters listed in the table.

Scheme 4

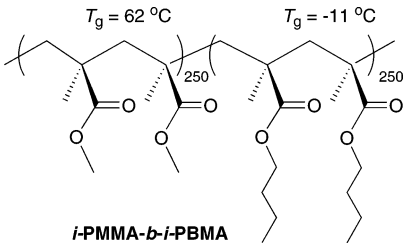

nonlinear regression graphical methods. First, the Fineman−Ross plot (Figure 6, left) of $X(1 - 1/Y)$ vs X^2/Y,

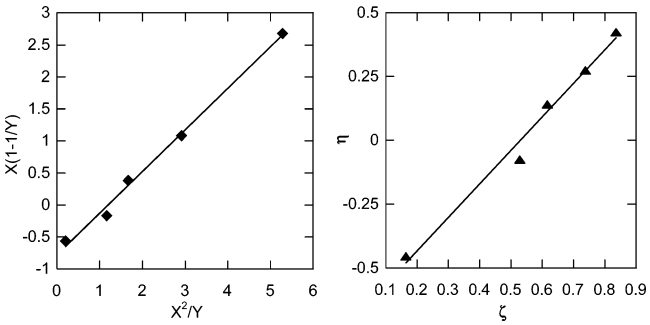

Figure 6. Fineman−Ross (left) and Kelen−Tüdõs (right) plots for the statistical copolymer P(MMA-*co*-BMA).

where X = [MMA]/[BMA] (monomer feed ratio) and Y = d[MMA]/d[BMA] (copolymer composition), yielded a straight line ($R^2 = 0.997$) with a slope of 0.65 and an intercept of −0.78, giving monomer reactivity ratios of $r_{MMA} = 0.65$ and $r_{BMA} = 0.78$. Second, the Kelen−Tüdõs plot (Figure 6, right) of η vs ξ, where $\eta = [X(Y - 1)/Y]/[\alpha + X^2/Y]$ and $\xi = (X^2/Y)]/[\alpha + X^2/Y]$ in which the parameter α serves to distribute the experimental data uniformly and symmetrically between the limits of 0 and 1 and is determined from $\alpha = [(X^2/Y)_{low}(X^2/Y)_{high}]^{1/2}$, yielded a straight line ($R^2 = 0.992$) with a slope of 1.31 and an intercept of −0.69; this plot gave $r_{MMA} = 0.62$ (i.e., the extrapolated intercept when $\xi = 1$) and $r_{BMA} = 0.72$ (i.e., the product of α and the extrapolated intercept when $\xi = 0$). The monomer reactivity ratios are less than unity for both monomers using both methods with the product of the ratios ($r_{MMA} \times r_{BMA}$) = 0.45 (the Kelen−Tüdõs method), indicating that there is a greater tendency for cross-propagation than for homopolymerization and that the copolymer formed instantaneously has a somewhat alternating character. It should be noted here that these reactivity ratios obtained using the cationic, chiral *ansa*-zirconocene ester enolate **1** are substantially different from those obtained by conventional free radical polymerization ($r_{MMA} = 0.93$, $r_{BMA} = 1.22$),[15] anionic polymerization ($r_{MMA} = 1.04$, $r_{BMA} = 0.81$),[15] group-transfer polymerization ($r_{MMA} = 1.76$, $r_{BMA} = 0.67$;[15] $r_{MMA} = 0.44$, $r_{BMA} = 0.26$),[16] and metallocene polymerization using $Cp_2ZrMe_2/B(C_6F_5)_3/ZnEt_2$ ($r_{MMA} = 1.20$, $r_{BMA} = 1.50$),[1d] reflecting the strong influence of the nature of the active propagating centers on the copolymerization and subsequently on the copolymer structure.

It is tempting to suggest that the observed somewhat alternating tendency in the copolymerization of MMA and BMA by **1** is consistent with the proposed polymerization mechanism outlined in Scheme 2. Specifically, in the rate-determining step (**B** + monomer → **A**), when the last added monomer is BMA (i.e., a butyl enolate **B**), the steric effects would argue that the associative displacement of the coordinated methyl ester moiety derived from the preceding MMA addition favors the incoming MMA over BMA. On the other hand, when the last added monomer is MMA (i.e., a methyl enolate **B**), the electronic effects would argue that the associative displacement of the coordinated butyl ester moiety favors the incoming BMA over MMA.

Isolation of the Single MMA Addition Product−Eight-Membered Ring Intermediate 4. According to the mechanism outline in Scheme 2, the intermediate (resting state) after each MMA addition is the proposed eight-membered-ring cationic zirconocene ester enolate structure (i.e., structure **B**). In attempts to isolate the cationic cyclic ester enolate **4** (Scheme 2), a complex designed for modeling the structure **B** to perform a check of its kinetic competence and hopefully obtain the crystal structure, we carried out stoichiometric reactions of the cationic zirconocene ester enolate **1**, which was generated in situ from the reaction of the neutral methyl zirconocene ester enolate **2** with $(C_6F_5)_3B{\cdot}THF$ (vide supra), and MMA under varied conditions of temperature, solvent, and order of reagent addition sequence. Serendipitously, one particular addition sequence led us to the discovery of direct addition reaction of MMA and the *neutral* methyl zirconocene enolate **2** to form single MMA addition product *rac*-(EBI)ZrMe[OC(OMe)=C(Me)CH_2C(Me_2)C(O^{i}Pr)=O] (**3**) (Scheme 5). Specifically, upon mixing **2** with MMA in a 1:1 ratio in CD_2Cl_2 at ambient temperature, a gradual disappearance of the MMA monomer (but without PMMA formation) was observed; a subsequent preparative scale reaction cleanly afforded the single MMA addition product **3**. In the presence of excess MMA, no further MMA additions took place after the first MMA addition to **2**, even with extended reaction times (24 h).

This reaction of direct MMA addition to the neutral **2** proceeds presumably via a more reactive resonance form of **2** (Scheme 5), which is consistent with the observation that this reaction occurs in noncoordinating polar solvents such as CH_2Cl_2 but not in toluene, even under elevated temperatures (>70 °C). An alternative pathway via a direct Diels−Alder cycloaddition of the ester enolate moiety at Zr to the free MMA molecule—which forms an ortho ester intermediate followed by ring rearrangements leading to **3**—is also possible; however, this pathway can hardly explain the observation that further MMA additions do not take place in the current system.

The structure of **3** was proposed on the basis of the spectroscopic and analytical characterizations (see Experimental Section), while many attempts to obtain its crystal structure were unsuccessful. Nevertheless, both ^1H and ^{13}C NMR spectra of **3** feature characteristic signals for a methyl zirconocene ester enolate structure

Scheme 5

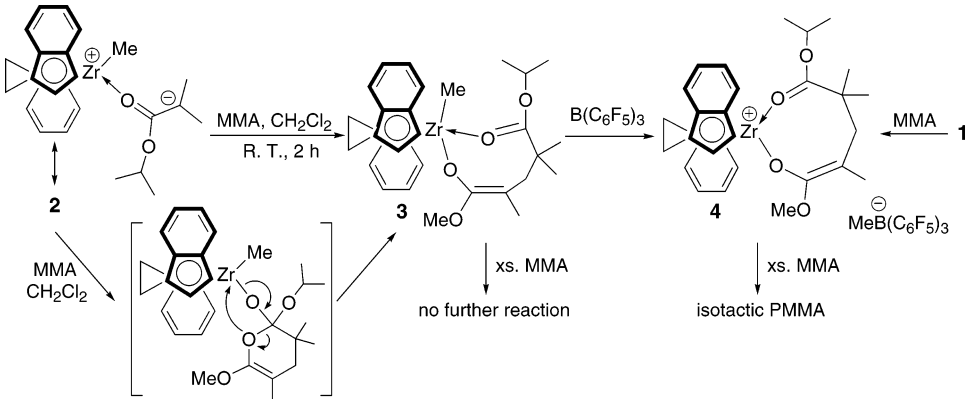

(which differs from that of the precursor **2**)[2a] and additionally an isopropyl ester group [−C(O^{i}Pr)=O]. Specifically, the ^{1}H NMR signal for −C*H*Me$_2$ (sept, 3.70 ppm) attached to the enolate ligand in **2** is substantially downfield shifted to 5.09 ppm (sept) for −C*H*Me$_2$ now attached to the ester group in **3**; the ^{13}C NMR chemical shift difference confirms these assignments: 153.88 ppm for the enolate *C*(O) carbon [(O*C*(O^{i}Pr)=] in **2** vs 177.65 ppm for the ester *C*(O) carbon [*C*(O^{i}Pr)=O] in **3**. In agreement with these spectroscopic changes on going from **2** to **3**, the added MMA now becomes a methyl ester enolate ligand [i.e., −OC(OMe)=C(Me)CH$_2$−] attached to Zr in **3**, which can be readily characterized by ^{1}H NMR [2.99 (O*Me*), 2.64 and 2.56 (C*H*$_2$), 1.41 (=C*Me*)] and by ^{13}C NMR {157.51[O*C*(OMe)=], 82.51 (=*C*Me), 54.31 (O*C*H$_3$), 42.35 (*C*H$_2$), 16.91 (=C*Me*)}.

The structure of **3** features a 5-coordinate Zr center (two Cp rings, two chelating oxygen atoms, and a methyl group; or a 9-coordinate Zr center considering a Cp ligand as 3-coordinate). A second set of minor resonances appears in ^{1}H NMR at temperature ≤−20 °C, presumably corresponding to a minor stereoisomer. It should be noted here that Sustmann and co-workers[7c] showed by computations that the addition of methyl acrylate to a methyl zirconocene ester enolate is feasible under suitable conditions while evaluating the possibility of a neutral monomeric polymerization mechanism and that such 5-coordinate neutral zirconocene structural motifs are not unusual.[17] The cyclic ring structure presented here for the current system can explain why no further MMA additions take place after the first MMA addition (i.e., formation of **3**) with both steric and electronic arguments. On the other hand, an alternative structure where the terminal ester group is not coordinated to Zr (i.e., the open chain structure) can hardly explain why further MMA additions do not proceed.

Another exciting aspect of this reaction—besides the direct addition of MMA to a neutral zirconocene ester enolate—is that the further reaction of **3** with $(C_6F_5)_3B\cdot$THF or B(C$_6$F$_5$)$_3$ at ambient temperature in CH$_2$Cl$_2$ cleanly produces the corresponding cationic zirconocene ester enolate species **4**, although complex **4** can also be obtained from the reaction of **1** and 1 equiv of MMA under suitable conditions (Scheme 5). Cationic cyclic ester enolate **4** is an isoelectronic structure of the neutral samarium complex (C$_5$Me$_5$)$_2$Sm(MMA)$_2$H, which has been isolated from the reaction of the samarium hydride precursor with 2 equiv of MMA and crystallographically characterized.[9] Two NMR spectroscopic characteristics of the isolated **4** are worth noting: first, as compared to the neutral precursor, the ^{13}C NMR resonance for the ester *C*(O) carbon [*C*(O^{i}Pr)=O] in **4** is substantially downfield shifted to 192.4 ppm (in CD$_2$Cl$_2$); this chemical shift value is nearly identical to that for the structurally characterized cationic complex where the *C*(O) oxygen is coordinated to the similar cationic zirconocene center (i.e., *rac*-(EBI)Zr$^+$(Me)OC(O^{i}Pr)OAl(C$_6$F$_5$)$_3^-$, albeit in a different NMR solvent: 190.2 ppm in C$_6$D$_6$),[2a] suggesting that the terminal isopropyl ester group is coordinated to the Zr$^+$ center. Second, the chemical shift for the methyl group in the [MeB(C$_6$F$_5$)$_3$]$^-$ anion is 0.54 ppm in CD$_2$Cl$_2$, which is nearly identical to that reported in the literature for the free [MeB(C$_6$F$_5$)$_3$]$^-$ anion (0.51 ppm in CD$_2$Cl$_2$).[18] The noncoordinating nature of the [MeB(C$_6$F$_5$)$_3$]$^-$ anion in **4** is also established by ^{19}F NMR in which a small chemical shift difference of <3 ppm [$\Delta(m,p$-F) = 2.7 ppm in **4**] between the *para*- and *meta*-fluorines is diagnostic of the noncoordinating [MeB(C$_6$F$_5$)$_3$]$^-$ anion.[18,19]

Much like the cationic species **1**, the cationic cyclic ester enolate **4** effects rapid further MMA additions leading to highly isotactic and high-molecular-weight PMMA. The significance of the isolated **4** is that it corresponds to the structure of the eight-membered-ring intermediate **B** after each C−C bond formation step, thereby providing further direct evidence supporting the proposed mechanism shown in Scheme 2.

Conclusions

Using the cationic, chiral *ansa*-zirconocene ester enolate complex, *rac*-(EBI)Zr$^+$(THF)[OC(O^{i}Pr)=CMe$_2$][MeB(C$_6$F$_5$)$_3$]$^-$ (**1**), which simulates the isospecific active propagating species **A** (Scheme 2) in the methacrylate polymerization by cationic, chiral *ansa*-zirconocene complexes, we have shown that the methacrylate polymerization by complex **1** is isospecific, living, and site-controlled, enabling the synthesis of highly isotactic homopolymers with narrow molecular weight distributions and block copolymers with well-defined structures.

The monomer reactivity ratios obtained from the statistical copolymerization of MMA and BMA by **1** differ substantially from those obtained using other types of active species, and the copolymer formed instantaneously by **1** has a somewhat alternating character. Kinetic studies of the MMA polymerization have shown that propagation is first order in both concentrations of the monomer and the active species, indicating a *monometallic*, intramolecular Michael addition propagation mechanism via the cyclic ester enolate intermediate **B** (Scheme 2), which was modeled by the isolated cationic cyclic ester enolate complex **4**. The results imply

that the resting state during a propagation "catalysis" cycle is the cyclic ester enolate **B** and associative displacement of the coordinated ester group by incoming methacrylate monomer to regenerate the active species **A** is the rate-determining step (i.e., **B** → **A**, Scheme 2).

The neutral methyl zirconocene ester enolate, *rac*-(EBI)ZrMe[OC(O^{i}Pr)═CMe$_2$] (**2**), can also undergo facile MMA addition in noncoordinating polar solvents, but the reaction is completely halted after the single MMA addition, forming the proposed structure **3**. However, when complex **3** is converted to the corresponding cationic species **4** upon addition of the borane abstractor, it rapidly and isospecifically adds more MMA to form high-molecular-weight PMMA. The significance of these reactions is at least twofold: first, the isolated cationic cyclic ester enolate **4** corresponds to the structure of the eight-membered-ring resting state **B** in a propagation "catalysis" cycle. Second, the observed unique, direct addition of MMA to the neutral ester enolate **2** opens a possibility of designing *neutral* group 4 metallocene enolate complexes as effective catalysts/initiators for polymerization of functionalized alkenes; research toward this goal is currently underway.

Acknowledgment. This work was supported by the National Science Foundation and Colorado State University. We thank Boulder Scientific Co. for the gift of B(C$_6$F$_5$)$_3$ and Profs. Scott Collins (U. of Akron), Rick Finke (CSU), and Tom Rovis (CSU) for helpful discussions. E.Y.C. acknowledges an Alfred P. Sloan Research Fellowship.

References and Notes

(1) By achiral zirconocenes: (a) Stojcevic, G.; Kim, H.; Taylor, N. J.; Marder, T. B.; Collins, S. *Angew. Chem., Int. Ed.* **2004**, *43*, 5523−5526. (b) Lian, B.; Toupet, L.; Carpentier, J.-F. *Chem.−Eur. J.* **2004**, *10*, 4301−4307. (c) Ferenz, M.; Bandermann, F.; Sustmann, R.; Sicking, W. *Macromol. Chem. Phys.* **2004**, *205*, 1196−1205. (d) Karanikolopoulos, G.; Batis, C.; Pitsikalis, M.; Hadjichristidis, N. *J. Polym. Sci., Part A: Polym. Chem.* **2004**, *42*, 3761−3774. (e) Wang, J.; Odian, G.; Haubenstock, H. *Polym. Prepr. (Am. Chem. Soc., Div. Polym. Chem.)* **2003**, *44*, 673−674. Wang, J.; Haubenstock, H.; Odian, G. *Polym. Prepr. (Am. Chem. Soc., Div. Polym. Chem.)* **2003**, *44*, 675−676. (f) Bandermann, F.; Ferenz, M.; Sustmann, R.; Sicking, W. *Macromol. Symp.* **2001**, *174*, 247−253. (g) Karanikolopoulos, G.; Batis, C.; Pitsikalis, M.; Hadjichristidis, N. *Macromolecules* **2001**, *34*, 4697−4705. (h) Bandermann, F.; Ferenz, M.; Sustmann, R.; Sicking, W. *Macromol. Symp.* **2000**, *161*, 127−134. (i) Shiono, T.; Saito, T.; Saegusa, N.; Hagihara, H.; Ikeda, T.; Deng, H.; Soga, K. *Macromol. Chem. Phys.* **1998**, *199*, 1573−1579. (j) Li, Y.; Ward, D. G.; Reddy, S. S.; Collins, S. *Macromolecules* **1997**, *30*, 1875−1883. (k) Deng, H.; Shiono, T.; Soga, K. *Macromol. Chem. Phys.* **1995**, *196*, 1971−1980. (l) Collins, S.; Ward, D. G. *J. Am. Chem. Soc.* **1992**, *114*, 5460−5462. (m) Farnham, W. B.; Hertler, W. U.S. Pat. 4,728,706, 1988.

(2) By chiral *ansa*-zirconocenes: (a) Bolig, A. D.; Chen, E. Y.-X. *J. Am. Chem. Soc.* **2004**, *126*, 4897−4906. (b) Strauch, J. W.; Fauré, J.-L.; Bredeau, S.; Wang, C.; Kehr, G.; Fröhlich, R.; Luftmann, H.; Erker, G. *J. Am. Chem. Soc.* **2004**, *126*, 2089−2104. (c) Chen, E. Y.-X.; Cooney, M. J. *J. Am. Chem. Soc.* **2003**, *125*, 7150−7151. (d) Karanikolopoulos, G.; Batis, C.; Pitsikalis, M.; Hadjichristidis, N. *Macromol. Chem. Phys.* **2003**, *204*, 831−840. (e) Batis, C.; Karanikolopoulos, G.; Pitsikalis, M.; Hadjichristidis, N. *Macromolecules* **2003**, *36*, 9763−9774. (f) See ref 1e. (g) Bolig, A. D.; Chen, E. Y.-X. *J. Am. Chem. Soc.* **2002**, *124*, 5612−5613. (h) Frauenrath, H.; Keul, H.; Höcker, H. *Macromolecules* **2001**, *34*, 14−19. (i) Bolig, A. D.; Chen, E. Y.-X. *J. Am. Chem. Soc.* **2001**, *123*, 7943−7944. (j) Cameron, P. A.; Gibson, V.; Graham, A. J. *Macromolecules* **2000**, *33*, 4329−4335. (k) Stuhldreier, T.; Keul, H.; Höcker, H. *Macromol. Rapid Commun.* **2000**, *21*, 1093−1098. (l) Chen, Y.-X.; Metz, M. V.; Li, L.; Stern, C. L.; Marks, T. J. *J. Am. Chem. Soc.* **1998**, *120*, 6287−6305. (m) Deng, H.; Shiono, T.; Soga, K. *Macromolecules* **1995**, *28*, 3067−3073. (n) Soga, K.; Deng, H.; Yano, T.; Shiono, T. *Macromolecules* **1994**, *27*, 7938−7940. (o) Collins, S.; Ward, D. G.; Suddaby, K. H. *Macromolecules* **1994**, *27*, 7222−7224.

(3) By achiral titanocenes: (a) Saegusa, N.; Shiono, T.; Ikeda, T.; Mikami, K. JP 10330391, 1998. (b) See ref 1m.

(4) By chiral *ansa*-titanocenes: (a) Jin, J.; Mariott, W. R.; Chen, E. Y.-X. *J. Polym. Chem., Part A: Polym. Chem.* **2003**, *41*, 3132−3142. (b) Jin, J.; Chen, E. Y.-X. *Organometallics* **2002**, *21*, 13−15.

(5) By half-sandwich titanium complexes: (a) Chen, E. Y.-X. *J. Polym. Sci., Part A: Polym. Chem.* **2004**, *42*, 3395−3403. (b) Jensen, T. R.; Yoon, S. C.; Dash, A. K.; Luo, L.; Marks, T. J. *J. Am. Chem. Soc.* **2003**, *125*, 14482−14494.

(6) By constraint geometry titanium and zirconium complexes: (a) Rodriguez-Delgado, A.; Mariott, W. R.; Chen, E. Y.-X. *Macromolecules* **2004**, *37*, 3092−3100. (b) Jin, J.; Chen, E. Y.-X. *Macromol. Chem. Phys.* **2002**, *203*, 2329−2333. (c) Jin, J.; Wilson, D. R.; Chen, E. Y.-X. *Chem. Commun.* **2002**, 708−709. (d) Nguyen, H.; Jarvis, A. P.; Lesley, M. J. G.; Kelly, W. M.; Reddy, S. S.; Taylor, N. J.; Collins, S. *Macromolecules* **2000**, *33*, 1508−1510.

(7) For computational studies, see: (a) Hölscher, M.; Keul, H.; Höcker, H. *Macromolecules* **2002**, *35*, 8194−8202. (b) Hölscher, M.; Keul, H.; Höcker, H. *Chem.−Eur. J.* **2001**, *7*, 5419−5426. (c) Sustmann, R.; Sicking, W.; Bandermann, F.; Ferenz, M. *Macromolecules* **1999**, *32*, 4204−4213.

(8) Sogah, D. Y.; Hertler, W. R.; Webster, O. W.; Cohen, G. M. *Macromolecules* **1987**, *20*, 1473−1488. (b) Webster, O. W.; Hertler, W. R.; Sogah, D. Y.; Farnham, W. B.; RajanBabu, T. V. *J. Am. Chem. Soc.* **1983**, *105*, 5706−5708.

(9) Yasuda, H.; Yamamoto, H.; Yamashita, M.; Yokota, K.; Nakamura, A.; Miyake, S.; Kai, Y.; Kanehisa, N. *Macromolecules* **1993**, *26*, 7134−7143. (b) Yasuda, H.; Yamamoto, H.; Yokota, K.; Miyake, S.; Nakamura, A. *J. Am. Chem. Soc.* **1992**, *114*, 4908−4909.

(10) Allen, R. D.; Long, T. E.; McGrath, J. E. *Polym. Bull. (Berlin)* **1986**, *15*, 127−134.

(11) Bovey, F. A.; Mirau, P. A. *NMR of Polymers*; Academic Press: San Diego, CA, 1996. (b) Chujo, R.; Hatada, K.; Kitamaru, R.; Kitayama, T.; Sato, H.; Tanaka, Y. *Polym. J.* **1987**, *19*, 413−424. (c) Ferguson, R. C.; Ovenall, D. W. *Polym. Prepr. (Am. Chem. Soc., Div. Polym. Chem.)* **1985**, *26*, 182−183. (d) Subramanian, R.; Allen, R. D.; McGrath, J. E.; Ward, T. C. *Polym. Prepr. (Am. Chem. Soc., Div. Polym. Chem.)* **1985**, *26*, 238−240.

(12) Odian, G. *Principles of Polymerization,* 3rd ed.; Wiley & Sons: New York, 1991; p 467.

(13) Fineman, M.; Ross, S. D. *J. Polym. Sci.* **1950**, *2*, 259−265.

(14) Kelen, T.; Tüdõs, F. *J. Macromol. Sci., Chem.* **1975**, *A9*, 1−27.

(15) Haddleton, D. M.; Crossman, M. C.; Hunt, K. H.; Topping, C.; Waterson, C.; Suddaby, K. G. *Macromolecules* **1997**, *30*, 3992−3998.

(16) Jenkins, A. D.; Tsartolia, E.; Walton, D. R. M.; Stejskal, J.; Kratochvil, P. *Polym. Bull. (Berlin)* **1988**, *20*, 97−100.

(17) For examples, see: (a) Hüsgen, N. S.; Luinstra, G. A.; Schaper, F.; Schmidt, K. *Inorg. Chem.* **1998**, *37*, 3471−3474. (b) Butchard, J.; Curnow, O. J.; Smail, S. J. *J. Organomet. Chem.* **1997**, *541*, 407−416. (c) Wang, Z.; Lu, S.; Guo, H. *Synth. React. Inorg. Metal-Org. Chem.* **1992**, *22*, 259−267. (d) Siedle, A. R.; Newmark, R. A.; Gleason, W. B.; Lamanna, W. M. *Organometallics* **1990**, *9*, 1290−1295.

(18) Klosin, J.; Roof, G. R.; Chen, E. Y.-X.; Abboud, K. A. *Organometallics* **2000**, *19*, 4684−4686.

(19) Horton, A. D.; de With, J.; van der Linden, A. J.; van de Weg, H. *Organometallics* **1996**, *15*, 2672−2674.

MA047345C